ELSEVIER

Physica D 99 (1996) 191–216

PHYSICA D

Large oscillations arising in a dispersive numerical scheme

C. David Levermore [a,*], Jian-Guo Liu [b,1]

[a] *Department of Mathematics, University of Arizona, Tucson, AZ 85721, USA*

[b] *Courant Institute of Mathematical Sciences, New York University, 251 Mercer Street, New York, NY 10012, USA*

Received 12 January 1996; revised 9 May 1996; accepted 9 May 1996

Communicated by A.C. Newell

Abstract

We study the oscillatory behavior that arises in solutions of a dispersive numerical scheme for the Hopf equation whenever the classical solution of that equation develops a singularity. Modulation equations are derived that describe period-two oscillations so long as the solution of those equations takes values for which the equations are hyperbolic. However, those equations have an elliptic region that may be entered by its solutions in a finite time, after which the corresponding period-two oscillations are seen to break down. This kind of phenomenon has not been observed for integrable schemes. The generation and propagation of period-two oscillations are asymptotically analyzed and a matching formula is found for the transition between oscillatory and nonoscillatory regions. Modulation equations are also presented for period-three oscillations. Numerical experiments are carried out that illustrate our analysis.

1. Introduction

In 1943 von Neumann used a central difference scheme to compute compressible fluid flows containing strong shocks and found oscillatory behavior after shock formation [30]. These oscillations arose due to the dispersive nature of the numerical scheme he chose and are characteristic of all such schemes. Many continuous analogs of this phenomenon have been studied recently – particularly in the context of the Korteweg–de Vries equation [6,20,28], the nonlinear Schrödinger equation [15], and the modified Korteweg–de Vries equation [5,15]. There have also been detailed studies of dispersive numerical schemes [7–13,19,24,26,29]. A review of many of these works can be found in [21].

In this paper we expand our original study [22] of the large oscillations arising in the numerical approximation of the Hopf (inviscid Burgers) initial-value problem

$$\partial_t u + u\partial_x u = 0, \qquad u(x,0) = u^{\mathrm{in}}(x), \tag{1.1}$$

* Corresponding author. E-mail: lvrmr@math.arizona.edu. Supported in part by NSF Grant DMS-8505550 while visiting the MSRI at Berkeley and by NSF Grant DMS-8914420.

[1] Current address: Department of Mathematics, Temple University, Philadelphia, PA 19122, USA.

Supported in part by NSF Grant DMS-8505550 as a postdoctoral fellow at the MSRI at Berkeley, by DOE Grant DE-FG02-88ER25053 as a visiting member at the Courant Institute, and by NSF Grant DMS-9505275.

PII S0167-2789(96)00157-1

given by the semidiscrete dispersive difference scheme

$$\frac{\mathrm{d}u_j}{\mathrm{d}t} + \tfrac{1}{3}(u_{j-1} + u_j + u_{j+1})\frac{u_{j+1} - u_{j-1}}{2h} = 0, \qquad u_j(0) = u^{\mathrm{in}}(x_j), \tag{1.2}$$

where $x_j = jh$ and $h = x_{j+1} - x_j$ is the spatial grid size. While the origin of this scheme is somewhat clouded, it has a long and distinguished history. For example, it was used by Zabusky and Kruskal [32] in 1965 when they discovered the remarkable interaction properties of soliton solutions of the Korteweg–de Vries equation. The historical appeal of this scheme derives from the fact that it possesses the two semidiscrete local conservation laws:

$$\frac{\mathrm{d}u_j}{\mathrm{d}t} + \frac{f_{j+1/2} - f_{j-1/2}}{h} = 0, \qquad f_{j+1/2} = \tfrac{1}{6}(u_j^2 + u_j u_{j+1} + u_{j+1}^2), \tag{1.3a}$$

$$\frac{\mathrm{d}u_j^2}{\mathrm{d}t} + \frac{g_{j+1/2} - g_{j-1/2}}{h} = 0, \qquad g_{j+1/2} = \tfrac{1}{3}(u_j^2 u_{j+1} + u_j u_{j+1}^2), \tag{1.3b}$$

hence reflecting the local conservation of u and u^2 by classical solutions of the Hopf equation (1.1).

Taylor expansion of the finite difference approximation (1.2) for small h allows its deviation from the Hopf equation (1.1) (i.e. its truncation error) to be read off from

$$\partial_t u + u\partial_x u + \tfrac{1}{18}h^2(u\partial_{xxx}u + \partial_{xxx}(u^2)) = \mathrm{O}(h^4). \tag{1.4}$$

Consequently, its continuum limit ($h \to 0$) has many similarities with the zero dispersion limit ($\varepsilon \to 0$) of the Korteweg–de Vries initial-value problem,

$$\partial_t u + u\partial_x u + \varepsilon^2\partial_{xxx}u = 0, \qquad u(x, 0) = u^{\mathrm{in}}(x), \tag{1.5}$$

which is a limit that has been well understood [20,28].

It is well known that for any initial data with a decreasing part the classical solution of the Hopf initial-value problem (1.1) develops an infinite derivative after a finite time, even if the initial data are smooth. So long as this solution remains classical, the solutions of both (1.2) and (1.5) will converge strongly to it as h or ε, respectively, tends to zero. As the singularity develops in the solution of (1.1), large oscillations develop in the approximating solutions of (1.2) and (1.5). It is known in the case of (1.5) that, as ε tends to zero, the wavelength of these oscillations is of order $\mathrm{O}(\varepsilon)$ while their amplitude does not vanish [20,28]. Solutions of the scheme (1.2) can exhibit similar behavior as h tends to zero. In either case, after the break time the solutions can at best be expected to have a weak limit as h or ε tends to zero.

This limiting behavior contrasts sharply with that for solutions of any zero dissipation limit, say as ε tends to zero in the Burgers initial-value problem:

$$\partial_t u + u\partial_x u - \varepsilon\partial_{xx}u = 0, \qquad u(x, 0) = u^{\mathrm{in}}(x). \tag{1.6}$$

In this case the solutions converge almost everywhere and strongly to a weak solution of (1.1) with shock discontinuities. After the formation of shocks this limiting solution locally dissipates u^2, a residual of the fact that the approximating solutions do so. On the other hand, u^2 is locally conserved by solutions of either (1.2) or (1.5). As a result, the weak limit of solutions of either (1.2) or (1.5), if it exists, cannot be this weak solution of the Hopf equation (1.1). Indeed, weak limits of solutions of (1.5) do not have shock discontinuities [20,28].

So far, much of the analysis of dispersive numerical schemes depends heavily on their integrability [1,2,11,16–19,26,29]. In fact, only a few integrable lattices have been studied in detail, those of Toda [2,26] and Kac–van Moerbeke [16], which are essentially identical, and that of Ablowitz–Ladik [1,18,19]. The study of near-integrable and nonintegrable numerical schemes is important for our general understanding of dispersive numerical phenomena.

We chose scheme (1.2) as prototypical (numerical evidence indicates that it is not integrable) and compare it with an integrable scheme. We find notable differences in the behavior of these two schemes.

The simplest oscillatory behavior is the period-two (or binary) oscillation, but even this exhibits many interesting phenomena that has made it the object of various numerical and theoretical studies [7,8,11–13,23,24,27,29]. In the spirit of the Whitham averaging method [31], we use the local conservation laws (1.3) to derive modulation equations that describe the evolution of an envelop of period-two oscillations. These modulation equations are identified as a central difference scheme for a 2×2 system which is strictly hyperbolic with a convex entropy in a region containing the initial data. As soon as the period-two oscillations evolve out of the hyperbolic region at some location, they break down locally while remaining a period-two oscillation elsewhere. The breakdown region exhibits chaotic small scale behavior, a phenomenon not observed in integrable schemes.

The organization of this paper is as follows. Section 2 treats the evolution of period-two oscillation in the dispersive numerical scheme (1.2). The conserved qualities are used to derive a system of modulation equations for period-two oscillations, which is found to have both hyperbolic and elliptic regions. We show by a Strang-type convergence analysis that the modulation equations give the limiting description of period-two oscillations so long their solution remains in the hyperbolic region and is sufficiently regular.

Section 3 studies the transition from nonoscillatory to period-two oscillatory behavior. We first present the onset of period-two oscillations in numerical experiments with the initial condition $u_0(x) = -\sqrt[3]{x}$, a generic case of shock formation, and a phase-plane analysis is made of the resulting self-similar behavior of the envelope of oscillations. We then present the onset of period-two oscillations in numerical experiments for rarefaction waves that continuously connect nonoscillatory to oscillatory solutions. In each case the onset of oscillations is found to propagate at the negative of the convection velocity. We use a weakly nonlinear asymptotic analysis to show that near the transistion between the nonoscillatory and oscillatory regions the oscillation envelop is described by a second Painlevé transcendent.

Section 4 studies the breakdown of period-two oscillations. First we show that as soon as the period-two oscillatory solution evolves into the elliptic region at some location, it breaks down locally while remaining a period-two oscillation wherever it stays in the hyperbolic region. In general, such a region of breakdown is not near a shock discontinuity. By the way of comparison, we consider the modulation of the period-two oscillations for an integrable scheme. We show that solutions of the corresponding modulation equations always lie in the hyperbolic region provided they do so initially. Numerical experiments illustrate that period-two oscillations do not break down for the integrable scheme. Finally, we illustrate by numerical experiment the sensitivity of period-two oscillations near a discontinuity to shifts in the computational grid.

In Section 5, we discuss the evolution of modulated period-three oscillations. Exact period-three oscillations evolve on a fast timescale, in contrast with the stationary character of period-two oscillations. Modulation equations for period-three oscillation are derived and analyzed; their solutions are compared with numerical experiments.

Finally, we give some concluding remarks in Section 6.

2. Evolution of period-two oscillations

2.1. Modulation equations for period-two oscillations

Due to its spatial central difference, the scheme (1.2) has exact stationary solutions with period-two spatial oscillations. Solutions in this family are determined up to a phase by their mean value v and mean square w which are defined by

$$v = \tfrac{1}{2}(u_j + u_{j+1}), \qquad w = \tfrac{1}{2}(u_j^2 + u_{j+1}^2). \tag{2.1}$$

The solution u_j is recovered (up to a phase) by

$$u_j = v \pm (-1)^j \sqrt{w - v^2}. \tag{2.2}$$

In order to describe a solution of (1.2) that is a modulation of this family of period-two oscillations it is therefore natural to introduce the variables

$$v_{j+1/2} = \tfrac{1}{2}(u_j + u_{j+1}), \qquad w_{j+1/2} = \tfrac{1}{2}(u_j^2 + u_{j+1}^2). \tag{2.3}$$

Both $v_{j+1/2}$ and $w_{j+1/2}$ are locally conserved densities of the scheme (1.2) and are smoothly varying for modulated period-two oscillations. The technique we use to derive modulation equations can be applied to many other dispersive numerical schemes [21]; it just requires that the scheme possesses a family of exact period-two solutions like (2.2) and at least two local conservation laws like (1.3).

The evolution of $v_{j+1/2}$ and $w_{j+1/2}$ can be simply expressed using the local conservation laws (1.3). First notice that the fluxes of (1.3) can be expressed in terms of the variables $v_{j+1/2}$ and $w_{j+1/2}$ as

$$f_{j+1/2} = \tfrac{1}{3}v_{j+1/2}^2 + \tfrac{1}{6}w_{j+1/2}, \qquad g_{j+1/2} = \tfrac{4}{3}v_{j+1/2}^3 - \tfrac{2}{3}v_{j+1/2}w_{j+1/2}. \tag{2.4}$$

Averaging the local conservation laws (1.3) over adjacent spatial points yields

$$\frac{\mathrm{d}v_{j+1/2}}{\mathrm{d}t} + \frac{f_{j+3/2} - f_{j-1/2}}{2h} = 0, \qquad \frac{\mathrm{d}w_{j+1/2}}{\mathrm{d}t} + \frac{g_{j+3/2} - g_{j-1/2}}{2h} = 0. \tag{2.5}$$

Eq. (2.5) can be viewed as the central difference approximation to the 2×2-system

$$\begin{aligned} &\partial_t v + \partial_x f(v, w) = 0, \qquad f(v, w) \equiv \tfrac{1}{3}v^2 + \tfrac{1}{6}w, \\ &\partial_t w + \partial_x g(v, w) = 0, \qquad g(u, v) \equiv \tfrac{4}{3}v^3 - \tfrac{2}{3}vw. \end{aligned} \tag{2.6}$$

Since $v_{j+1/2}$ and $w_{j+1/2}$ are smoothly varying for modulated period-two oscillations, formally at least, their continuum limits v and w will satisfy (2.6), the so-called modulation equations for period-two oscillations. Furthermore, v and w are then the weak limits of u_j and u_j^2, respectively.

The Jacobian matrix of the flux functions of (2.6) is

$$A = \begin{pmatrix} \partial_v f & \partial_w f \\ \partial_v g & \partial_w g \end{pmatrix} = \frac{1}{6}\begin{pmatrix} 4v & 1 \\ 24v^2 - 4w & -4v \end{pmatrix}, \tag{2.7}$$

and its eigenvalues are

$$\lambda_\pm = \pm\tfrac{1}{3}\sqrt{10v^2 - w}. \tag{2.8}$$

Clearly, system (2.6) is hyperbolic in the region

$$\{(v, w) \mid w < 10v^2\}, \tag{2.9}$$

and is elliptic in the region

$$\{(v, w) \mid 10v^2 \leq w\}. \tag{2.10}$$

It can be shown that classical solutions of the modulation equations (2.6) satisfy

$$\partial_t(w - v^2) - v\partial_x(w - v^2) - \tfrac{2}{3}(w - v^2)\partial_x v = 0. \tag{2.11}$$

Hence, the region $v^2 \leq w$ is invariant for these solutions, a fact that is consistent with the origins (2.3) of v and w and indeed allows the reconstruction of u (up to phase) through formula (2.2). However, as we demonstrate in the next section, the hyperbolic region is not invariant for these solutions.

If the initial data are nonoscillatory then $w - v^2$ will be zero initially and by (2.11) will remain zero so long as the solution of (2.6) is classical. The characteristic velocity associated with $w - v^2$ is seen to be $-v$, the negative of the convective velocity associated with v. This means the onset of period-two oscillations will propagate with velocity $-v$ into a nonoscillating region. This fact will be seen again later in the paper, both in analyses of the behavior of special solutions, and through a linearized analysis of nonoscillatory solutions.

2.2. *Persistence and stability of period-two oscillations*

In Section 2.1 we derived the averaged conservation laws (2.4) and (2.5) and showed that they were a central difference scheme to the system of modulation equations (2.6). Here we justify, at least in some cases, the formal passage to the continuum limit, thereby establishing the persistence and stability of the oscillations.

The Strang convergence theorem [25] states that if a solution of a nonlinear hyperbolic system is sufficiently smooth and the linearization of a numerical scheme which approximates that solution is L^2 stable then the scheme for the nonlinear problem is strongly convergent. We will use a variant of this result. We consider the system of hyperbolic conservation laws

$$\partial_t U + \partial_x F(U) = 0, \qquad U(x,0) = U^{\text{in}}(x), \tag{2.12}$$

where $U = U(t,x)$ has period one in x and takes values in $\mathbb{R}^d$. The flux $F(U)$ is assumed to be a smooth function from $\mathbb{R}^d$ into itself with a Jacobian $\nabla_U F(U)$ that can be smoothly diagonalized within the reals as

$$\nabla_U F(U) = L^{-1}(U)\Lambda(U)L(U).$$

Here $\Lambda(U)$ is the diagonal matrix of (real) eigenvalues of $\nabla_U F(U)$ and $L(U)$ is the matrix of corresponding left eigenvectors. We consider the semidiscrete central difference scheme

$$\frac{\mathrm{d}U_j}{\mathrm{d}t} + \frac{F(U_{j+1}) - F(U_{j-1})}{2h} = 0, \qquad U_j(0) = U^{\text{in}}(x_j), \tag{2.13}$$

where $h = 1/j$ and $x_j = jh$ for some positive integer J. We show that this scheme is linearly L^2 stable and, hence, has full accuracy if the solution of (2.12) is sufficiently smooth.

Theorem 2.1. Let $U = U(x,t)$ be a C^3 solution of (2.12) of period one in x with (C^3) initial data $U^{\text{in}}(x)$. Let $U_j^{(J)}(t)$ be the solution of (2.13) for $h = 1/J$. Then for $0 < t < T$ we have

$$\sqrt{\frac{1}{J}\sum_{j=1}^{J} |U(x_j,t) - U_j^{(J)}(t)|^2} \le C\frac{1}{J^2}. \tag{2.14}$$

Proof. Since U has C^3 regularity one has

$$\frac{\mathrm{d}U(x_j,t)}{\mathrm{d}t} + \frac{F(U(x_{j+1},t)) - F(U(x_{j-1},t))}{2h} = \mathrm{O}(h^2). \tag{2.15}$$

Denote the error by $E_j(t) = U_j(t) - U(x_j,t)$. Now we suppose a priori that

$$\max_j\{|E_j(t)|\} \le h \quad \text{for } 0 < t < t_0. \tag{2.16}$$

If we apply this supposition then the Taylor expansion of F about $U(x_j)$ gives

$$F(U_j) - F(U(x_j)) = \nabla_U F(U(x_j))E_j + \tfrac{1}{2}\nabla_U^2 F(U(x_j))E_jE_j + \mathrm{O}(h^3), \tag{2.17}$$

where the t-dependence has been suppressed. When (2.15) is subtracted from (2.13) and (2.17) is employed, one obtains

$$\frac{\mathrm{d}E_j}{\mathrm{d}t} + \frac{\nabla_U F(U(x_{j+1}))E_{j+1} - \nabla_U F(U(x_{j-1}))E_{j-1}}{2h} = -\frac{1}{2}\frac{\nabla_U^2 F(U(x_{j+1}))E_{j+1}E_{j+1} - \nabla_U^2 F(U(x_{j-1}))E_{j-1}E_{j-1}}{2h} + \mathrm{O}(h^2). \tag{2.18}$$

Now introduce the notation

$$\Lambda_j = \Lambda(U(x_j)), \qquad L_j = L(U(x_j)), \qquad V_j = L_j E_j,$$

and express (2.18) as

$$\begin{aligned}\frac{\mathrm{d}V_j}{\mathrm{d}t} &+ \frac{\Lambda_{j+1}V_{j+1} - \Lambda_{j-1}V_{j-1}}{2h} \\ &= \frac{\mathrm{d}L_j}{\mathrm{d}t}L_j^{-1}V_j - \frac{1}{2}L_j\frac{\nabla_U^2 F(U(x_{j+1}))E_{j+1}E_{j+1} - \nabla_U^2 F(U(x_{j-1}))E_{j-1}E_{j-1}}{2h} \\ &\quad - L_j\frac{(L_{j+1}^{-1} - L_j^{-1})\Lambda_{j+1}V_{j+1} - (L_{j-1}^{-1} - L_j^{-1})\Lambda_{j-1}V_{j-1}}{2h} + \mathrm{O}(h^2) \\ &= \mathrm{O}(|V_{j+1}| + |V_{j-1}|) + \mathrm{O}(h^2).\end{aligned}$$

Take the scalar product of this equation with V_j, sum by parts, and again use supposition (2.16) to obtain

$$\frac{\mathrm{d}}{\mathrm{d}t}\sum_{j=1}^{J}|V_j|^2 \le C\sum_{j=1}^{J}|V_j|^2 + \mathrm{O}(h^3).$$

When integrated in time, this yields

$$\sum_{j=1}^{J}|V_j(t)|^2 \le \mathrm{O}(h^3) \quad \text{for } t < t_0,$$

or equivalently,

$$\sum_{j=1}^{J}|E_j(t)|^2 \le \mathrm{O}(h^3) \quad \text{for } t < t_0. \tag{2.19}$$

The Cauchy–Schwarz inequality then implies

$$\max_j\{|E_j(t)|\} \le \mathrm{O}(h^{3/2}) \quad \text{for } t < t_0.$$

The a prori assumption (2.16) is therefore justified for $t < t_0$. With a standard continuity argument one concludes

$$\sum_{j=1}^{J}|U_j(t) - U(x_j, t)|^2 \le C_T h^3 \quad \text{for } 0 \le t \le T.$$

Because $= 1/J$, this establishes the theorem. □

We now apply Theorem 2.1 to our system of modulation equations (2.6) to obtain our main result.

Theorem 2.2. Let $(v, w) = (v(x,t), w(x,t))$ be a C^3 solution of the modulation equations (2.6) of period one in x with (C^3) initial data $(v^{\rm in}(x), w^{\rm in}(x))$ that satisfies $v^{\rm in2} \le w^{\rm in} < 10v^{\rm in2}$. Let $u_j^{(J)}(t)$ be the solution of scheme (1.2) satisfying the initial condition

$$u_j^{(J)}(0) = v^{\rm in}(x_j) + (-1)^j \sqrt{w^{\rm in}(x_j) - v^{\rm in}(x_j)^2}. \tag{2.20}$$

Upon defining $v_{j+1/2}^{(J)}(t)$ and $w_{j+1/2}^{(J)}(t)$ in terms of $u_j^{(J)}(t)$ by (2.3), then for $0 < t < T$ we have

$$\sqrt{\frac{1}{J}\sum_{j=1}^{J}\left(|v(x_{j+1/2},t) - v_{j+1/2}^{(J)}(t)|^2 + |w(x_{j+1/2},t) - w_{j+1/2}^{(J)}(t)|^2\right)} \le C\frac{1}{J}, \tag{2.21}$$

where $x_{j+1/2} = (j + \frac{1}{2})h$.

Proof. From definition (2.3) of $v_{j+1/2}^{(J)}(0)$ and a $w_{j+1/2}^{(J)}(0)$ in terms of the initial data $u_j^{(J)}(0)$ given by (2.20), one can at best conclude that

$$v_{j+1/2}^{(J)}(0) = v^{\rm in}(x_{j+1/2}) + \mathrm{O}(h), \qquad w_{j+1/2}^{(J)}(0) = w^{\rm in}(x_{j+1/2}) + \mathrm{O}(h). \tag{2.22}$$

The result then follows from Theorem 2.1 and the Lipschitz dependence of the solution on initial data. □

Remark. The rate of convergence given by (2.21) is not as fast as that given by (2.14), however, convergence was all we were after.

3. Onset of period-two oscillations

3.1. Self-similar onset

As stated in Section 1, large oscillations develop in the solutions of (1.2) when the corresponding classical solution of the Hopf initial-value problem (1.1) develops an infinite derivative. The generic behavior of a Hopf solution at the instant an infinite derivative develops is that of a cube root singularity. To study the onset of oscillations, it is therefore natural to consider scheme (1.2) with the initial data

$$u^{\rm in}(x) = -x^{1/3}. \tag{3.1}$$

One advantage of discrete problems is that numerical simulations can be used to give a general picture of the problem. Indeed, our analysis is guided by careful numerical experiments [23]. We begin by reviewing those experiments for the initial data (3.1). We will show that period-two oscillations develop in the solution of (1.2) which fan out from a jump-discontinuity at $x = 0$ in a self-similar fashion.

In Figures 1(a)–(b), we plot the numerical solutions of scheme (1.2) with initial data (3.1) for a grid size of $h = 0.01$ at times $t = 0.0$, $t = 0.3$, $t = 0.6$ and $t = 0.9$, respectively. Eq. (1.2) was solved using an Adams–Bashforth method with the time step equal to $0.2h$. The numerical boundary condition was implemented by imposing the endvalues at every time step. We also used a four-step Rung–Kutta method to solve (1.2) and obtained indistinguishable results. The evident discontinuity in the envelope of period-two oscillations at the center of Fig. 1(b) does not correspond to a shock solution of the modulation equations (2.6), but rather to a contact discontinuity because there is no flux

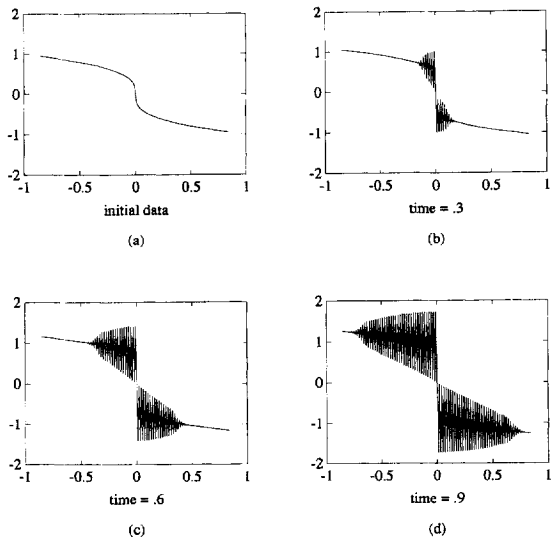

Fig. 1. Numerical solutions of the dispersive scheme (1.2) approximating the Hopf equation (1.1) with initial data $u^{\text{in}}(x) = -\sqrt[3]{x}$ at: (a) $t = 0$; (b) $t = 0.3$; (c) $t = 0.6$; (d) $t = 0.9$.

across it. System (2.6) has zero as a double characteristic at this point and, hence, is not strictly hyperbolic. This degeneracy will be examined in Section 4.3. Figs. (a)–(d) clearly show that the envelope of period-two oscillations fans out in both direction from this discontinuity as the time increases. The envelope is smooth except at the origin and at the points where the oscillatory region connects to the nonoscillatory solution with a square root profile.

For comparison we consider the zero-dissipation solution of the Hopf equation, say obtained in the limit of vanishing ε of solutions of (1.6) with initial data (3.1). It can be shown that this solition is self-similar and has the form

$$u(x,t) = t^{1/2} f\left(\frac{x}{t^{3/2}}\right),$$

where $f = f(\xi)$ satisfies

$$f(\xi) - 3\xi f'(\xi) + 2f(\xi)f'(\xi) = 0, \qquad f(\xi) \sim -\xi^{1/3} \quad \text{as } |\xi| \to \infty. \tag{3.2}$$

This can be integrated to find the relation $\xi = -f^3 + f$. This then determines f uniquely for $\xi^2 > \frac{4}{27}$, while for $\xi^2 \leq \frac{4}{27}$ it must be augmented by the "equal area rule" to determine which value of f is selected [31]. The solution is found to possess a jump discontinuity (a shock) at $\xi = 0$ for any positive time. In Fig. 2 this solution, obtained with an ENO scheme, is compared to the weak limit of the numerical solutions that were presented in Fig. 1. Since those solutions were modulations of period-two oscillations, their weak limit is computed accurately by averaging values at adjacent spatial points. We can see in Fig. 2 that the weak limit of the numerical solution of the scheme (1.2) is not equal to the zero-dissipation solution of Hopf equation (1.1) in the oscillatory region. The difference between them is small but increases with time.

It is apparent from Fig. 1. that, like the zero-dissipation solution of the Hopf equation, the envelope of oscillations might be self-similar. Indeed, it is easy to check that the numerical scheme (1.2) has a similarity: namely, that if we let $u_j^h(t)$ denotes its solution for grid size h then

$$u_j^h(t) = \frac{1}{\alpha} u_j^{\alpha^3 h}(\alpha^2 t) \quad \text{for every } \alpha > 0. \tag{3.3}$$

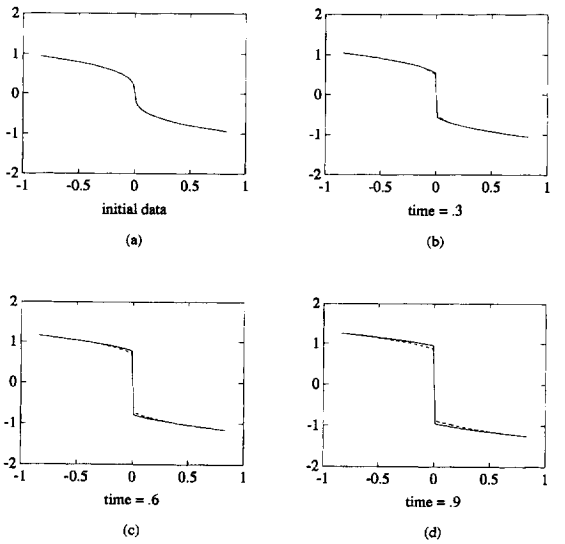

Fig. 2. The solid lines are the zero-dissipation solution of the Hopf equation (1.1) at: (a) $t = 0$; (b) $t = 0.3$; (c) $t = 0.6$; (d) $t = 0.9$. The dashed lines indicate the weak limit of the dispersive scheme (1.2) as computed from the same solution shown in Fig. 1. The difference between them is small but increases with time.

This symmetry gives rise to a self-similar solution for the envelope equations (2.6). In order to analyze this self-similarity, we bring the equations into a more symmetric form by introducing the transformation

$$v = \tfrac{1}{2}(a+b), \qquad w = \tfrac{1}{2}(a^2+b^2), \tag{3.4}$$

so that the modulation equation equations (2.6) become

$$\partial_t a + \tfrac{1}{3}(a+2b)\partial_x b = 0, \qquad \partial_t b + \tfrac{1}{3}(b+2a)\partial_x a = 0. \tag{3.5}$$

In light of (2.2), a and b can be thought of as the envelope of the oscillations. This form of the modulation equations can be derived directly from the scheme (1.2) and is similar to that used by Goodman and Lax [7] in the context of their discretization.

A self-similar solution of (3.5) takes the form

$$a(x,t) = t^{1/2} g\left(\frac{x}{t^{3/2}}\right), \qquad b(x,t) = t^{1/2} k\left(\frac{x}{t^{3/2}}\right),$$

where $g = g(\xi)$ and $k = k(\xi)$ satisfy

$$3g - 9\xi g' + 2(g+2k)k' = 0, \qquad 3k - 9\xi k' + 2(k+2g)g' = 0. \tag{3.6}$$

In order to recover the nonoscillatory initial data (3.1), the solution of (3.6) should satisfy the boundary condition

$$g(\xi) = k(\xi) = f(\xi) \quad \text{for } |\xi| \text{ large enough}, \tag{3.7}$$

where $f = f(\xi)$ solves $\xi = -f^3 + f$ just as for the zero-dissipation limit. This ensures that the zero-dispersion limit agrees with the zero-dissipation limit where the former has no oscillations.

The scaling homogeneity of (3.6) indicates that this system can be transformed into an essentially autonomous system by introducing

$$\xi g_1(\xi) = g(\xi), \qquad \xi k_1(\xi) = k(\xi). \tag{3.8}$$

Then (3.6) becomes

$$\begin{aligned}\xi\frac{dg_1}{d\xi} &= 2\frac{-27g_1+3(g_1+2k_1)k_1+2(g_1+2k_1)(2g_1+k_1)g_1}{81-4(g_1+2k_1)(k_1+2g_1)},\\ \xi\frac{dk_1}{d\xi} &= 2\frac{-27k_1+3(k_1+2g_1)g_1+2(k_1+2g_1)(2k_1+g_1)k_1}{81-4(g_1+2k_1)(k_1+2g_1)}.\end{aligned} \tag{3.9}$$

The behavior if (g_1, k_1) can now be studied through a phase-plane analysis.

For the initial data (3.1) the self-similar profiles g and h will be odd functions of ξ that are positive for $\xi < 0$. The functions g_1 and k_1 defined in (3.8) will therefore be even functions of ξ that are nonpositive. The corresponding orbit of (3.9) will then lie entirely in the third quadrant of the (g_1, k_1)-plane. By the even symmetry in ξ, it suffices to consider only $\xi < 0$. It is clear that by (3.7) the solution of (3.8) satisfies

$$g_1(\xi) = k_1(\xi) = f(\xi)/\xi \sim -\xi^{-2/3} \quad \text{as } \xi \to -\infty. \tag{3.10}$$

The vector field of (3.9) is singular along the hyperbola

$$81 - 4(g_1 + 2k_1)(k_1 + 2g_1) = 0 \tag{3.11}$$

with the exception of the point $(g_1, k_1) = (-\frac{3}{2}, -\frac{3}{2})$ where the numerators on the right-hand side of (3.9) both vanish too. Therefore, as ξ increases from $-\infty$, the solution of (3.9) moves along the line $g_1 = k_1$ from the origin towards the hyperbola (3.11), passing through it at $(-\frac{3}{2}, -\frac{3}{2})$, its only regular point. There are many orbits emanating from this point on the other side of the hyperbola, but only one of them gives a solution for which $g(\xi)$ tends to zero as $\xi \to 0$. To get on this orbit, the solution of (3.9) develops a singularity, turning abruptly to the left at $(-\frac{3}{2}, -\frac{3}{2})$ then proceeds to asymptotically approach the vertical line $g_1 = -\frac{3}{2}$. This singularity corresponds to the onset of oscillations in the numerical solution of (1.2).

Let ξ_0 denote the value of ξ at this singular point. By (3.10)

$$f_0 \equiv f(\xi_0) = g_1(\xi_0)\xi_0 = -\tfrac{3}{2}\xi_0, \tag{3.12}$$

where f_0 satisfies $\xi_0 = -f_0^3 + f_0$. Whence,

$$\xi_0 = -\tfrac{2}{3}\left(\tfrac{5}{3}\right)^{1/2}, \qquad f_0 = \left(\tfrac{5}{3}\right)^{1/2}. \tag{3.13}$$

In the original variables this singularity happens at (x_0, u_0) where

$$x_0(t) = \xi_0 t^{3/2} = -\tfrac{2}{3}\left(\tfrac{5}{3}\right)^{1/2} t^{3/2}, \qquad u_0(t) = u(x_0(t), t) = f_0 t^{1/2} = \left(\tfrac{5}{3}\right)^{1/2} t^{1/2}. \tag{3.14}$$

Clearly,

$$\frac{dx_0(t)}{dt} = -\left(\tfrac{5}{3}\right)^{1/2} t^{1/2} = -u(x_0(t), t). \tag{3.15}$$

The above equality tell us that the onset of the oscillations propagates at the negative of the convection velocity. As we indicated before, this is generally true. In the next section, this phenomenon will be examined through a linear analysis.

The above phase-plane analysis can be illustrated with numerical experiments. In Fig. 3 the numerical results from Fig. 1(b) are replotted in the (g_1, k_1)-phase plane. The values of g_1 and k_1 are computed by averaging adjacent points of the numerical solution in the self-similar scale and dividing by the grid location jh. It is clear in Fig. 3 that the computed values of (g_1, k_1) lie along the line $g_1 = k_1$ from the origin toward the hyperbola, passing close to the point $(-\frac{3}{2}, -\frac{3}{2})$, and then, as is seen in Fig. 4, asymptote to the line $g_1 = -\frac{3}{2}$ as $\xi \to 0$. This is consistent with the foregoing phase-plane analysis of (3.9), the directional vector-field of which is indicated with arrows in Fig. 3.

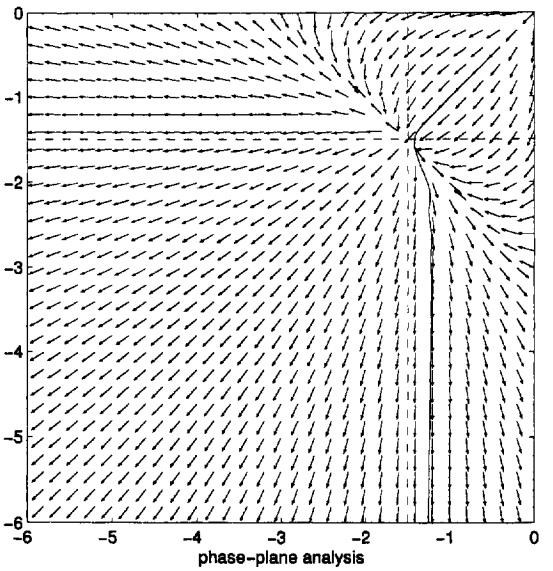

Fig. 3. The directional vector-field of (3.9) in the (g_1, k_1)-plane is indicated with arrows. The envelope of the $t = 0.3$ oscillations seen in Fig. 1(b) is shown here as a superimposed dark solid line.

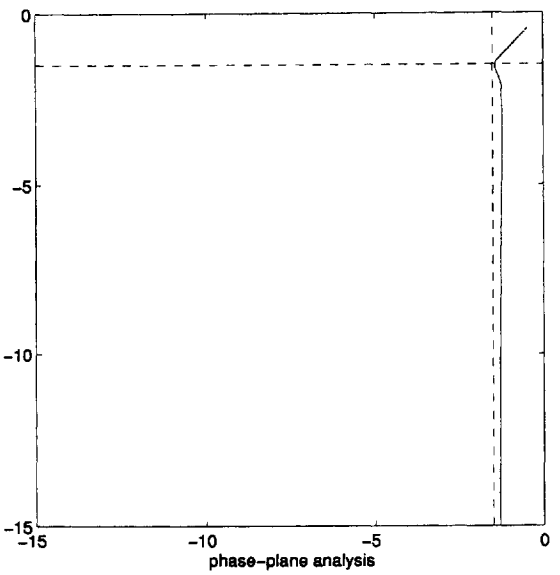

Fig. 4. The same as Fig. 3, but without the arrows and on a scale that more clearly illustrates the slow asympotic approach to the line $g_1 = -\frac{3}{2}$ as $\xi \to 0$.

3.2. *Onset for rarefaction waves*

We now consider those rarefaction wave solutions of the modulation equations (2.6) that make a continuous transition from a uniform nonoscillatory to a uniform oscillatory state. Specifically, for any $\bar{u}$ and $\xi_c > 0$ we

consider initial data of (2.6) in the form

$$(v^{\mathrm{in}}(x), w^{\mathrm{in}}(x)) = \begin{cases} (\bar{u}, \bar{u}^2) & \text{for } x \le 0, \\ (v^{\mathrm{R}}(x), w^{\mathrm{R}}(x)) & \text{for } 0 < x < \xi_{\mathrm{c}}, \\ (v^{\mathrm{R}}(\xi_{\mathrm{c}}), w^{\mathrm{R}}(\xi_{\mathrm{c}})) & \text{for } \xi_{\mathrm{c}} \le x, \end{cases} \tag{3.16}$$

where $(v, w) = (v^{\mathrm{R}}(\xi), w^{\mathrm{R}}(\xi))$ is the solution of the rarefaction wave profile equation

$$\frac{\mathrm{d}}{\mathrm{d}\xi}\begin{pmatrix} v \\ w \end{pmatrix} = \begin{pmatrix} r_1(v, w) \\ r_2(v, w) \end{pmatrix}, \qquad \begin{pmatrix} v \\ w \end{pmatrix}\Big|_{\xi=0} = \begin{pmatrix} \bar{u} \\ \bar{u}^2 \end{pmatrix}, \tag{3.17}$$

for the right eigenvector $(r_1, r_2)^{\mathrm{T}}$ corresponding to the eigenvalue $\lambda = -\frac{1}{3}\sqrt{10v^2 - w}$ of the coefficient matrix (2.7) given by

$$\begin{pmatrix} r_1(v, w) \\ r_2(v, w) \end{pmatrix} = \frac{3\sqrt{10v^2 - w}}{12v + \sqrt{10v^2 - w}} \begin{pmatrix} 1 \\ 4v + 2\sqrt{10v^2 - w} \end{pmatrix}. \tag{3.18}$$

Here the eigenvector $(r_1, r_2)^{\mathrm{T}}$ has been normalized so that $(r_1, r_2) \cdot (\partial_v \lambda, \partial_w \lambda) \equiv 1$.

The rarefaction wave solutions of the modulation equations (2.6) corresponding to the initial data (3.16) is then

$$(v(x,t), w(x,t)) = \begin{cases} (\bar{u}, \bar{u}^2) & \text{for } x \le -\bar{u}t, \\ (v^{\mathrm{R}}(\xi), w^{\mathrm{R}}(\xi)) & \text{for } -\bar{u}t < x < \xi_{\mathrm{c}} + (\xi_{\mathrm{c}} - \bar{u})t, \\ (v^{\mathrm{R}}(\xi_{\mathrm{c}}), w^{\mathrm{R}}(\xi_{\mathrm{c}})) & \text{for } \xi_{\mathrm{c}} + (\xi_{\mathrm{c}} - \bar{u})t \le x. \end{cases} \tag{3.19}$$

where

$$\xi \equiv \frac{x + \bar{u}t}{1 + t}.$$

The onset of oscillations is again seen to propagate with velocity $-\bar{u}$.

We now consider the solution of (1.2) with initial data given by

$$u_j(0) = v^{\mathrm{in}}(x_j) + (-1)^j \sqrt{w^{\mathrm{in}}(x_j) - v^{\mathrm{in}}(x_j)^2}. \tag{3.20}$$

The profile is computed numerically from the ODE (3.17). These initial data are plotted in Fig. 5(a). The corresponding numerical solution of (1.2) at $t = 0.5$ is presented in Fig. 5(b). It shows that the period-two oscillation has persisted and propagated. To show clearly that this propagation is a rarefaction behavior, in Figs. 5(c) and (d) we plot the data of (a) and (b), respectively, in the (v, w)-plane. The initial data in Fig. 5(c) are the Rankine curve determined by (3.17). As excepted, the data viewed in the (v, w)-plane at a later time, plotted in (d) for $t = 0.5$, are the same as for the initial curve in (c). This indicates that the solution is the rarefaction wave.

3.3. *Weakly nonlinear analysis of onset*

Points where the microscopic behavior of the numerical solution changes from oscillatory to nonoscillatory can be thought of as the location of a phase transition in the sense of nonequilibrium statistical mechanics. Near such a point the amplitude of the oscillations is small, so that the transition may be studied through a weakly nonlinear asymptotic analysis.

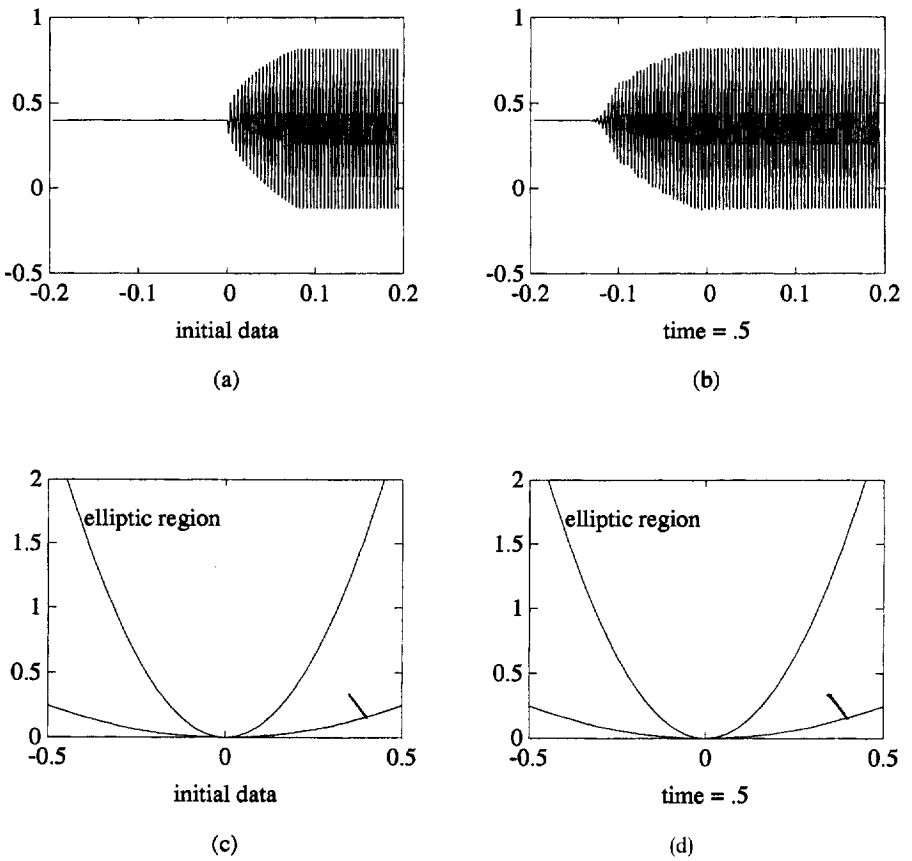

Fig. 5. The initial data shown in (a) are the rarefaction data (3.16). (b) The solution of (1.2) at $t = 0.5$. (c) The initial data in the (v, w)-plane consist of the rarefaction curve given by (3.17). The endpoint on the curve $w = v^2$ represents the nonoscillatory left-hand state, while the other endpoint represents the oscillatory right-hand uniform state. (d) The solution at $t = 0.5$ in the (v, w)-plane is a curve that is almost identical with the initial curve in (c).

When the difference scheme (1.2) is linearized about a constant value $u = \bar{u}$, one obtains

$$\frac{du_j}{dt} + \bar{u}\frac{u_{j+1} - u_{j-1}}{2h} = 0. \tag{3.21}$$

Seeking solutions of the form $u_j(t) = \exp(i(\kappa x_j - \omega t))$, one finds that the dispersion relation $\omega = \omega(\kappa)$ and group velocity $c = c(\kappa)$ are given by

$$\omega(\kappa) = \frac{\bar{u}}{h}\sin(\kappa h), \qquad c(\kappa) \equiv \frac{d\omega}{d\kappa}(\kappa) = \bar{u}\cos(\kappa h). \tag{3.22}$$

The general use of the group velocity to analyze dispersive numerical schemes is discussed in [27]. A stationary phase analysis of the Fourier integral representation of the solution as $h \to 0$ shows that the dominant signals will propagate at the critical values of the group velocity, the so-called characteristic velocities. For (3.22) these are $c_\pm \equiv c(\kappa_\pm) = \pm\bar{u}$, which are attained at the wave numbers $\kappa_+ = 0$ and $\kappa_- = \pi/h$ and have the frequencies $\omega_\pm = 0$. These linear modes are

$$u_j(t) = 1, \qquad u_j(t) = (-1)^j, \tag{3.23}$$

and are also the basis for the set of exact stationary period-two solutions upon which the modulation equations (2.6) are based. In other words, the velocity $\bar{u}$ corresponds to smooth information while $-\bar{u}$ corresponds to period-two oscillations.

Since period-two oscillations propagate with the fastest group velocity, the oscillatory behavior at a leading edge of the transition region is basically composed of weak period-two oscillations. It is easily checked that if (v_j, z_j) satisfy

$$\begin{aligned} &\frac{\mathrm{d}v_j}{\mathrm{d}t} + \tfrac{1}{3}(v_{j+1} + v_j + v_{j-1})\frac{v_{j+1} - v_{j-1}}{2h} + \tfrac{1}{3}(z_{j+1} - z_j + z_{j-1})\frac{z_{j+1} - z_{j-1}}{2h} = 0, \\ &\frac{\mathrm{d}z_j}{\mathrm{d}t} + \tfrac{1}{3}(v_{j+1} + v_j + v_{j-1})\frac{z_{j+1} - z_{j-1}}{2h} - \tfrac{1}{3}(z_{j+1} - z_j + z_{j-1})\frac{v_{j+1} - v_{j-1}}{2h} = 0, \end{aligned} \tag{3.24}$$

then $u_j = v_j + (-1)^j z_j$ solves (1.2). We will therefore construct approximate solutions of (1.2) by first constructing approximate solutions of (3.24).

In order to study small fluctuations about a nonzero homogeneous state $u = \bar{u}$, we introduce $\bar{v}$ and $\bar{z}$ by

$$v_j \equiv \bar{u} + h^2 \bar{v}_j, \qquad z_j \equiv h\bar{z}_j. \tag{3.25}$$

Then setting this into (3.24) yields

$$\begin{aligned} &\frac{\mathrm{d}\bar{v}_j}{\mathrm{d}t} + \bar{u}\frac{\bar{v}_{j+1} - \bar{v}_{j-1}}{2h} + \tfrac{1}{3}(\bar{z}_{j+1} - \bar{z}_j + \bar{z}_{j-1})\frac{\bar{z}_{j+1} - \bar{z}_{j-1}}{2h} \\ &\quad + h^2 \tfrac{1}{3}(\bar{v}_{j+1} + \bar{v}_j + \bar{v}_{j-1})\frac{\bar{v}_{j+1} - \bar{v}_{j-1}}{2h} = 0, \end{aligned} \tag{3.26a}$$

$$\begin{aligned} &\frac{\mathrm{d}\bar{z}_j}{\mathrm{d}t} - \bar{u}\frac{\bar{z}_{j+1} - \bar{z}_{j-1}}{2h} - h^2 \tfrac{1}{3}(\bar{v}_{j+1} + \bar{v}_j + \bar{v}_{j-1})\frac{\bar{z}_{j+1} - \bar{z}_{j-1}}{2h} \\ &\quad - h^2 \tfrac{1}{3}(\bar{z}_{j+1} - \bar{z} + \bar{z}_{j-1})\frac{\bar{v}_{j+1} - \bar{v}_{j-1}}{2h} = 0. \end{aligned} \tag{3.26b}$$

Now suppose that the values of $\bar{v}_j$ and $\bar{z}_j$ are approximated by point evaluations of smooth spatial functions that are slowly varying in the frame moving with velocity $-\bar{u}$. Introduce the smooth functions $v = v(s, y)$ and $z = z(s, y)$ such that

$$\bar{v}_j(t) \sim v(x_j + \bar{u}t, h^2 t), \qquad \bar{z}_j(t) \sim z(x_j + \bar{u}t, h^2 t). \tag{3.27}$$

After setting (3.27) into (3.26) and Taylor expanding in h one finds

$$2\bar{u}\partial_y v + \tfrac{1}{3} z \partial_y z = \mathrm{O}(h^2), \tag{3.28a}$$

$$\partial_s z - \tfrac{1}{6}\bar{u}\partial_y^3 z - v\partial_y z - \tfrac{1}{3} z \partial_y v = \mathrm{O}(h^2). \tag{3.28b}$$

Upon integrating (3.28a) to leading order, one finds

$$v = -\frac{1}{12}\frac{1}{\bar{u}} z^2 + C. \tag{3.29}$$

If this solution is to extend into a nonoscillatory region where the perturbation vanishes, we must impose the boundary conditions $v = z = 0$ there; hence $C = 0$. When this result is substituted back into (3.28b) it yields to leading order

$$\partial_s z - \frac{1}{6}\bar{u}\partial_y^3 z + \frac{5}{36}\frac{1}{\bar{u}} z^2 \partial_y z = 0. \tag{3.30}$$

Therefore, the amplitude z of the oscillations in the phase transition region approximately satisfies the modified Korteweg–deVries equation (3.30). Given any smooth solution $z = z(y, s)$ of (3.30), an approximate solution of (1.2) may be constructed in the form

$$u_j(t) = \bar{u} + (-1)^j z(x_j + \bar{u}t, h^2 t)h - \frac{1}{12}\frac{1}{\bar{u}}(z(x_j + \bar{u}t, h^2 t))^2 h^2 + \mathrm{O}(h^3). \tag{3.31}$$

The shift $x_j + \bar{u}t$ on the right-hand side of the above formula again tells us that the onset of oscillations propagates with velocity $-\bar{u}$.

The general form of (3.31) can also be obtained from the classical theory of continuous weak solutions with jump discontinuities in the spatial first derivatives [3]. Specifically, when the jump in the first derivative of a continuous solution of a quasilinear first-order hyperbolic system lies along a differentiable curve in the (x, t)-plane then the discontinuity propagates at a characteristic velocity and the jump is a corresponding right eigenvector of the coefficient matrix. To apply this result, the modulation equations (2.6) are recast yet again as

$$\partial_t \begin{pmatrix} v \\ q \end{pmatrix} + \begin{pmatrix} v & \frac{1}{6} \\ -\frac{2}{3}q & -v \end{pmatrix} \partial_x \begin{pmatrix} v \\ q \end{pmatrix} = 0, \tag{3.32}$$

where v is as before, and $q = w - u^2$. One sees from (2.2) that regions where $q = 0$ correspond to nonoscillatory regions of the modulational solution. At a boundary between such a nonoscillatory region and an envelope of oscillations where (3.32) has a continuous weak solution with value $(\bar{u}, 0)$, the discontinuity propagates at velocity $-\bar{u}$ and the coefficient matrix evaluated at $(v, q) = (\bar{u}, 0)$ has a corresponding right eigenvector $(-\frac{1}{12}(1/\bar{u}),\ 1)^{\mathrm{T}}$. Behind the discontinuity the solution of (3.32) therefore takes the form

$$\begin{pmatrix} v \\ q \end{pmatrix} \sim \begin{pmatrix} \bar{u} \\ 0 \end{pmatrix} + h^2\phi^2 \begin{pmatrix} -\frac{1}{2}(1/\bar{u}) \\ 1 \end{pmatrix} \tag{3.33}$$

for some amplitude function ϕ^2. Recovering u_j from formula (2.2) gives

$$u_j = v + (-1)^j\sqrt{q} \sim \bar{u} + (-1)^j h\phi - \frac{1}{12}\frac{1}{\bar{u}}h^2\phi^2, \tag{3.34}$$

which has the exact same form as (3.31). The jump discontinuity in the derivative of ϕ^2 means that the envelope of oscillations connects to the nonoscillatory region of value $\bar{u}$ with a square root profile. This observation generalizes what we had seen in the rarefaction problem of Section 3.2.

The following theorem establishes the validity of expansion (3.27) for initial data with small amplitude period-two oscillations.

Theorem 3.1. Let $z = z(y, s)$ be a smooth periodic solution of (3.30) with initial data $z_0 = z_0(x)$. Let $u_j(t)$ be the solution of (1.2) with initial data

$$u_j(0) = \bar{u} + (-1)^j z_0(x_j)h - \frac{1}{12}\frac{1}{\bar{u}}(z_0(x_j))^2 h^2, \tag{3.35}$$

and $\tilde{u}_j(t)$ be the approximation

$$\tilde{u}_j(t) = \bar{u} + (-1)^j z(x_j + \bar{u}t, h^2 t)h - \frac{1}{12}\frac{1}{\bar{u}}(z(x_j + \bar{u}t, h^2 t))^2 h^2. \tag{3.36}$$

Then one has the L^2-estimate

$$\sqrt{\frac{1}{J}\sum_{j=1}^{J} |u_j(t) - \tilde{u}_j(t)|^2} = \mathrm{O}(h^3), \tag{3.37}$$

where the estimate is uniform over any compact interval of t.

Proof. Define the error by $e_j(t) = \tilde{u}_j(t) - u_j(t)$. Setting this into scheme (1.2) yields

$$\frac{de_j}{dt} + \tfrac{1}{3}(\tilde{u}_{j+1} + \tilde{u}_j + \tilde{u}_{j-1})\frac{e_{j+1} - e_{j-1}}{2h} + \tfrac{1}{3}(e_{j+1} + e_j + e_{j-1})\frac{\tilde{u}_{j+1} - \tilde{u}_{j-1}}{2h} + \tfrac{1}{3}(e_{j+1} + e_j + e_{j-1})\frac{e_{j+1} - e_{j-1}}{2h} = T_j(z), \tag{3.38}$$

where the truncation error $T_j(z)$ satisfies the L^2 estimate

$$\sum_j (T_j(z))^2 h \le Ch^6. \tag{3.39}$$

Multiply Eq. (3.38) by e_j and use the local conservation property (1.3b) to obtain

$$\frac{1}{2}\frac{d}{dt}e_j^2 + \tfrac{1}{3}(\tilde{u}_{j+1} + \tilde{u}_j + \tilde{u}_{j-1})\frac{e_{j+1}e_j - e_je_{j-1}}{2h} + \tfrac{1}{3}e_j(e_{j+1} + e_j + e_{j-1})\frac{\tilde{u}_{j+1} - \tilde{u}_{j-1}}{2h} + \frac{1}{3}\frac{e_j^2e_{j+1} + e_je_{j+1}^2 - e_{j-1}^2e_j - e_{j-1}e_j^2}{h} = e_jT_j(z). \tag{3.40}$$

Now sum over j and use summation by parts leads to

$$\frac{1}{2}\frac{d}{dt}\sum_j e_j^2 - \sum_j e_je_{j+1}\frac{\tilde{u}_{j+2} - \tilde{u}_{j-1}}{3h} + \frac{1}{3}\sum_j e_j(e_{j+1} + e_j + e_{j-1})\frac{\tilde{u}_{j+1} - \tilde{u}_{j-1}}{2h} = \sum_j e_jT_j(z). \tag{3.41}$$

Notice that from (3.36) that

$$\tilde{u}_j - \tilde{u}_{j+1} = O(h).$$

One sees from (3.41) that

$$\frac{d}{dt}\sum_j e_j^2 \le C\sum_j (T_j(z)^2 + e_j^2). \tag{3.42}$$

The Gronwall inequality and truncation estimate (3.39) then yields

$$\sum_j e_j^2 h \le e^{Ct}\sum_j T_j^2 h \le O(h^6). \tag{3.43}$$

This completes the proof of the theorem. □

Remark. The idea used in Theorem 3.1 can be generalized to systems with strictly convex entropy function when the numerical scheme has the same entropy function.

In the numerical experiments in Sections 3.1 and 3.2 we saw that the envelop of oscillations connects with the nonoscillatory region with a parabolic curve. We now give an explanation. Assume that the solution of (3.30) has the following self-similar form:

$$Z(y, s) = \frac{1}{\alpha\sqrt[3]{\alpha s}} f\left(\frac{\beta y}{\sqrt[3]{\alpha s}}\right), \tag{3.44}$$

where

$$\beta = \frac{5^{1/8}}{\bar{u}^{1/2}}, \qquad \alpha = \tfrac{1}{6}\bar{u}\beta^3. \tag{3.45}$$

By plugging the above into (3.30) and scaling the coefficients, we obtain

$$f + \xi f_\xi - f_{\xi\xi\xi} + 6f^2 f_\xi = 0. \tag{3.46}$$

This equation can be integrated once to find

$$f_{\xi\xi} = 2f^3 + \xi f + \gamma \tag{3.47}$$

for some constant γ. Eq. (3.47) is the Painlevé equation of the second kind, whose solution is the second Painlevé transcendent [14]. One can see by directly analyzing (3.47) as $\xi \to \infty$ that f has the asymptotic behavior

$$f(\xi) \sim \sqrt{\xi}. \tag{3.48}$$

Hence, by (3.44),

$$Z(y,s) \sim \frac{1}{\alpha\sqrt[3]{\alpha s}}\sqrt{\frac{\beta y}{\sqrt[3]{\alpha s}}} = \frac{1}{\alpha}\sqrt{\frac{\beta y}{\alpha s}} = \sqrt{\frac{6^3\bar{u}}{5}}\sqrt{\frac{y}{s}}.$$

Therefore, we have from (3.31) that

$$u_j(t) \sim \bar{u} + (-1)^j\sqrt{\frac{6^3\bar{u}}{5}}\sqrt{\frac{x_j + \bar{u}t}{t}} + O(h).$$

This shows that the period-two oscillation in the phase-transition region matches the outside large oscillations in a parabolic curve, thereby recovering (3.34).

The above analysis is consistent with the numerical experiments in Sections 3.1 and 3.2. As we have showed analytically in (2.24) and numerically in Figs. 1 and 5, oscillations propagate into a nonoscillatory region with a velocity that is the negative of the convection velocity. Period-two oscillations that mark the transition from nonoscillatory to oscillatory behavior are described by the second Painlevé transcendent that matches to a parabolic envelope.

4. Breakdown of period-two oscillations

4.1. Loss of hyperbolicity for period-two oscillations

The following numerical experiment illustrates what happens when a period-two oscillation evolves into the elliptic region (2.10) at some location [23]. We consider scheme (1.2) with the initial data

$$u^{\text{in}}(x) = -0.3\sin(\pi x). \tag{4.1}$$

Clearly, singularities will form in the solution of the Hopf equation (1.1) when $t = 1$ at $x = 0, \pm 1, \pm 2, \ldots$. For a grid size $h = 0.005$, we plot the numerical solution at $t = 6$, $t = 11$ and $t = 12$ in Figs. 6(a)–(c), respectively. The ODE (1.2) is solved using the Adams–Bashforth method with the CFL number equal to 0.2.

The discontinuity in the envelope of period-two oscillations at the center of Fig. 6(a) is again a contact discontinuity (with no flux across it). The period-two oscillations are generated at the central contact discontinuity and fan out

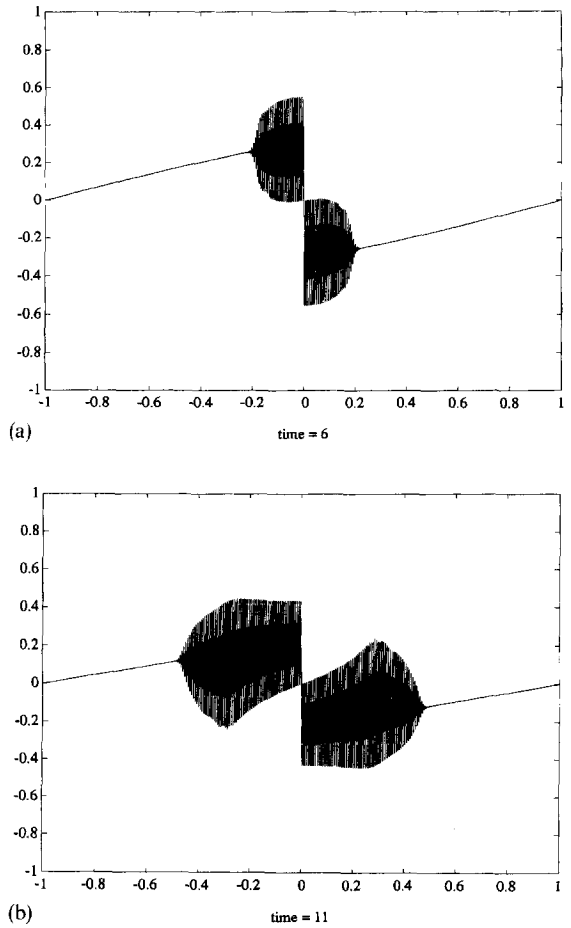

Fig. 6. (a) The solution of the scheme (1.2) with initial data $u^{\text{in}}(x) = -0.3\sin(\pi x)$ at $t = 6$. The grid size is $h = 0.005$. The solution develops period-two oscillations when the solution of the Hopf equation (1.1) develops a singularity. Their envelope fans out as time increases and has a contact discontinuity at the origin.
(b) A continuation of the solution shown in Fig. 6(a) to $t = 11$. The period-two oscillations have evolved to a point where their envelop has just left the hyperbolic region (2.9). Notice the slight irregularity in the oscillations near $x = \pm 0.3$ where the hyperbolicity condition has just been violated.
(c) A continuation of the solution shown in Figs. 6(a) and (b) to $t = 12$. The envelope of period-two oscillations has broken down, and a spatially and temporally chaotic region has developed. Notice that a well-defined region of period-two oscillations persists.

in both directions as time increases. The oscillations are slowly varying in space and time, and their envelope is smooth expect at the central contact discontinuity and at the endpoints of the oscillating region where the envelope has a square root behavior. Fig. 6(b) shows the growth of the oscillatory region and the development of two small defects in the envelope at $x \sim 0.3$ where the solution has just moved out of the hyperbolic region (2.9). The resulting dramatic local breakdown of the period-two oscillations is shown in Fig. 6(c), where the solution is seen to remain a perfect period-two oscillation throughout much of space. Within the breakdown region the solution becomes rapidly varying in both space and time, behaving in a chaotic way. Notice that this breakdown occurs far from the central contact discontinuity. In order to ensure that this phenomenon is not simply generated by the numerical ODE solver, we halved the time step and obtained indistinguishable results. We believe that Fig. 6(c) depicts the dynamical behavior of ODE (1.2). Our numerical evidence was inconclusive regarding the question of whether or not a weak

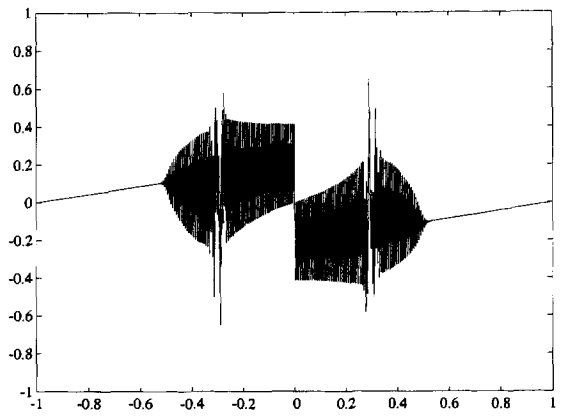

Fig. 6. Continued

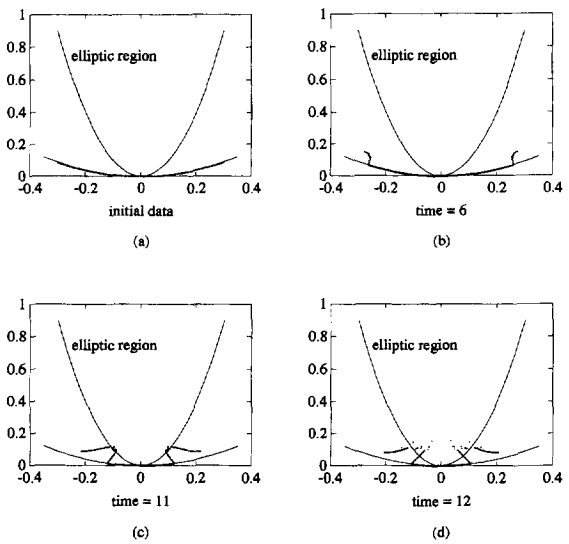

Fig. 7. The same solution of scheme (1.2) that was shown in Figs. 6(a)–(c) is depicted here in the (v, w)-plane. The initial data (a) lie on the curve $w = v^2$. At $t = 6$ (b) the solution lies completely within the hyperbolic region(2.9). At $t = 11$ (c) it has just crossed the curve $w = 10v^2$, thereby entering the elliptic region (2.10) and triggering the local breakdown of period-two oscillations. At $t = 12$ (d) the solution is well into the elliptic region and the period-two oscillations have broken down. Near the boundary curve $w = 10v^2$, parts of the solution maintain a period-two structure even in the elliptic region.

limit exists in this region. Indeed, given the complexity of the observed dynamics, it would seem that convincing evidence on the matter could only be obtained from much larger experiments.

To further illustrate this connection between the local loss of hyperbolicity and the breakdown of the modulated period-two solutions, in Figs. 7(b)–(d) we depict the solution of Figs. 6(a)–(c) in the (v, w)-plane. The initial data in Fig. 7(a) lie on the curve $w = v^2$. As the period-two oscillations are developed, Fig. 7(b) shows that the solution enters the hyperbolic region (2.9). At $t = 11$, Fig. 7(c) shows that the solution has just passed the curve $w = 10v^2$ and entered the elliptic region (2.10). While the breakdown time of the period-two oscillations is seen to coincide with the time, the solution enters the elliptic region, notice in Fig. 7(d) that some period-two structure persists into the elliptic region. The cause for this persistent structure is not well understood.

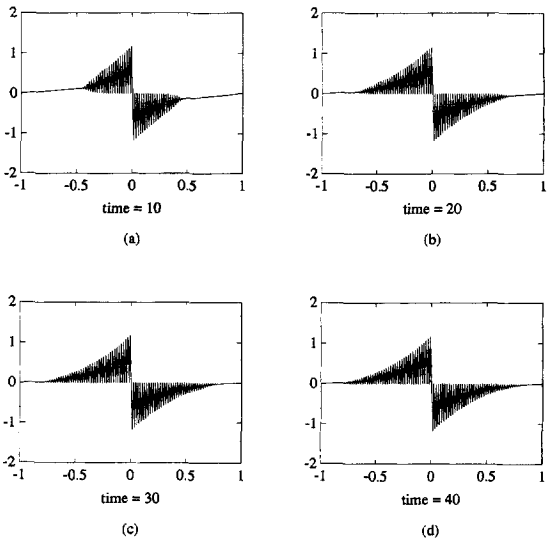

Fig. 8. The solution of the integrable scheme (4.2) (the Kac–Moerbeke lattice) with initial data $u^{\text{in}}(x) = -0.3\sin(\pi x)$ at: (a) $t = 10$; (b) $t = 20$; (c) $t = 30$; (d) $t = 40$. The grid size is $h = 0.01$. The solution develops period-two oscillations when the solution of the Hopf equation (1.1) develops a singularity. Their envelope fans out as time increases and has a contact discontinuity at the origin. Unlike the solution of the nonintegrable scheme shown in Figs. 6(a)–(c), here the period-two oscillations never break down.

4.2. *Comparison with an integrable scheme*

The breakdown of period-two oscillations in this way has not been observed in integrable schemes. For comparison, we approximate the Hopf equation (1.1) with initial data (4.1) by the dispersive scheme

$$\frac{\mathrm{d}u_j}{\mathrm{d}t} + u_j \frac{u_{j+1} - u_{j-1}}{2h} = 0, \qquad u_j(0) = u^{\text{in}}(x_j), \tag{4.2}$$

and plot the numerical solutions at times $t = 10$, $t = 20$, $t = 30$ and $t = 40$ in Figs. 8(a)–(d), respectively. The above scheme were shown by Goodman and Lax [7] to be equivalent to the Kac–von Moerbeke lattice [16], provided the initial data have same sign, and hence are integrable. They used the variables

$$u_j = \tfrac{1}{2}(a_j + b_j) + (-1)^j \tfrac{1}{2}(a_j - b_j) \tag{4.3}$$

to describe the period-two oscillations and obtained the following modulation equations:

$$\partial_t a + a\partial_x b = 0, \qquad \partial_t b + b\partial_x a = 0. \tag{4.4}$$

As in Section 2.1, we use two conserved qualities to rederive the modulation equation of the period-two oscillations. Being integrable, (4.2) has infinitely many conservation laws. We chose the following two conservation laws to derive the modulation equations:

$$\frac{\mathrm{d}(\log|u_j|)}{\mathrm{d}t} + \frac{u_{j+1} - u_{j-1}}{2h} = 0, \qquad \frac{\mathrm{d}u_j}{\mathrm{d}t} + \frac{u_j u_{j+1} - u_{j-1}u_j}{2h} = 0. \tag{4.5}$$

We define the following two variables which is enough to determine the period-two oscillations:

$$v_{j+1/2} = \tfrac{1}{2}(u_j + u_{j+1}), \qquad w_{j+1/2} = -\tfrac{1}{2}(\log|u_j| + \log|u_{j+1}|). \tag{4.6}$$

Indeed, we can recover the oscillatory solution u_j by

$$u_j = v_{j+1/2} \pm (-1)^j \sqrt{v_{j+1/2}^2 - \exp(-2w_{j+1/2})},$$

We have from (4.5) and (4.6) that

$$\frac{\mathrm{d}w_{j+1/2}}{\mathrm{d}t} - \frac{v_{j+3/2} - v_{j-1/2}}{2h} = 0, \qquad \frac{\mathrm{d}v_{j+1/2}}{\mathrm{d}t} + \frac{1}{2}\frac{\mathrm{e}^{-2w_{j+3/2}} - \mathrm{e}^{-2w_{j-1/2}}}{2h} = 0. \tag{4.7}$$

This is the modulation equation for the period-two oscillations of scheme (4.2) and indeed it is just Toda lattice. We can also view (4.7) as the central difference scheme for the following p-system with exponential law:

$$\partial_t w - \partial_x v = 0, \qquad \partial_t v + \tfrac{1}{2}\partial_x e^{-2w} = 0 \tag{4.8}$$

with initial data

$$(v, w)|_{t=0} = (u_0(x), -\log u_0(x)).$$

By convexity, we known that the solution can only appear in the following region:

$$\{(v, w) \mid w \geq -\log|v|\}. \tag{4.9}$$

Clearly, system (4.8) is always strictly hyperbolic in the above region. This differs from the modulation equations (2.6) of the nonintegrable scheme (1.2) which can change type.

The relation between the stability of numerical schemes and their integrability was also studied by Herbst and Ablowitz [10] through a finite difference approximation to the cubic Schrödinger equation. They found that the standard central difference scheme (which is nonintegrable) could induce numerical chaos in the solution while an integrable scheme (obtained through a minor modification in the approximation of the cubic term) performs better. Of course, some integrable systems have elliptic modulation equations, but we know of no integrable systems with modulation equations that dynamically change type as was shown for Eqs. (2.6).

4.3. A phase instability in period-two oscillations

The contact discontinuity in the solution of the modulation equations that arises at the origin in the last two experiments is a delicate point. We now illustrate the instability of the solution at that point to fractional shifts of the grid. The above two numerical experiments are reperformed with the computational grid points $x_j = (j + \alpha)h$, where $0 < \alpha < 1$ and $\alpha \neq 0.5$. The initial data will then no longer have an odd symmetry with respect to the grid. The initial data used in Figs. 9 and 10 are the same as that used in Figs. 1 and 6, respectively, except that the grid has been shifted by choosing $\alpha = \sqrt{2} - 1$, a negligible amount on the continuum scale.

Figures 9 and 10 clearly demonstrate again that the period-two oscillations generated at the origin fan out as time increases. In Fig. 9 the period-two oscillations persist but develop a long wavelength modulation. However, in Fig. 10 the period-two oscillations are destroyed in a region near the origin that also fans out as time increases. The period-two oscillations always move fastest, and so are found furthest from the origin. Notice that the dramatic behavior characteristic of entering the elliptic region in Figs. 6(b)–(c) also appears in Figs. 10(c)–(d).

It was shown above that wherever the modulation equations (2.6) are strictly hyperbolic their classical solutions describe period-two oscillations that are insensitive to shifts in the underlying grid. Hence, the differences seen in the corresponding runs above are generated at the contact discontinuity located at the origin and then propagate out from there. This indicates a grid-scale sensitivity on the initial data.

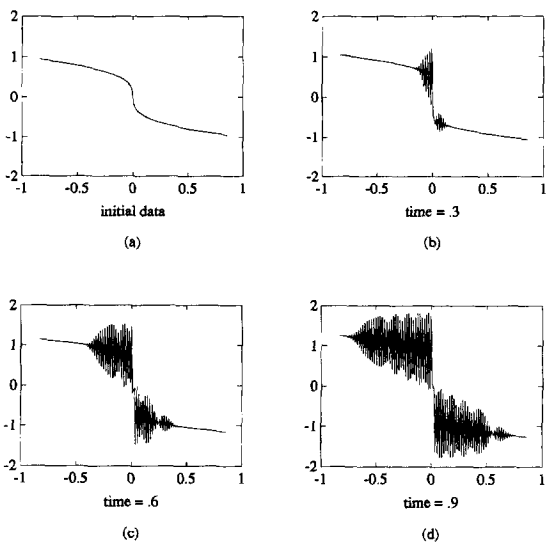

Fig. 9. The solution of the scheme (1.2) for the same initial data as in Fig. 1 except that the grid is shifted by $(\sqrt{2}-1)h$. The odd symmetry is therefore broken, and while still composed of period-two oscillations, structure is formed on long wavelengths.

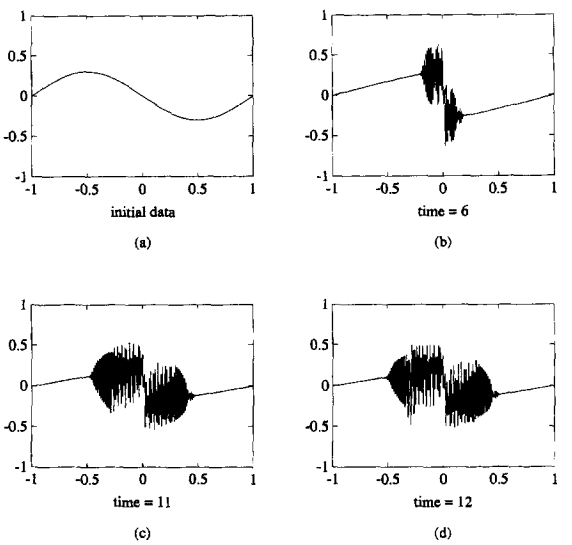

Fig. 10. The solution of the scheme (1.2) for the same initial data as in Fig. 6 except that the grid is shifted by $(\sqrt{2}-1)h$. The odd symmetry is therefore broken, and the solution is no longer composed solely of period-two oscillations.

5. Modulation of period-three oscillations

Of course, oscillatory behavior in the solution of a dispersive numerical scheme is generally not period-two in nature. One might therefore consider making a more general Whitham ansatz of the form

$$u = U(t, x, \theta(t, x)/h), \tag{5.1}$$

where $\theta(t, x)$ is some smooth function. However, the discrete nature of the computational grid is not consistent with such an ansatz because on fine scales there is not a continuum of wave numbers available to the solution. We shall therefore consider a more modest extension of the preceding theory – namely to period-three oscillations.

The period-three oscillations are very different from period-two oscillations because, while exact period-two oscillations are stationary, exact period-three oscillations vary rapidly in time. Here, we derive modulation equations for period-three oscillations through by averaging the local conservation laws (1.3).

Exact period-three solutions are completely determined by (u_0, u_1, u_2), which will sastisfy the three-particle version of system (1.2), namely

$$\frac{\mathrm{d}}{\mathrm{d}t}\begin{pmatrix} u_0 \\ u_1 \\ u_2 \end{pmatrix} = -\frac{1}{3}\frac{u_0+u_1+u_2}{2h}\begin{pmatrix} 0 & 1 & -1 \\ -1 & 0 & 1 \\ 1 & -1 & 0 \end{pmatrix}\begin{pmatrix} u_0 \\ u_1 \\ u_2 \end{pmatrix}. \tag{5.2}$$

Since the quantity $u_0 + u_1 + u_2$ is conserved by solution of (5.2), denoting its value by $3\bar{a}$, the general solution of this system may be expressed as

$$\begin{pmatrix} u_0(t) \\ u_1(t) \\ u_2(t) \end{pmatrix} = \exp\left(-\frac{t\bar{a}}{2h}M\right)\begin{pmatrix} u_0(0) \\ u_1(0) \\ u_2(0) \end{pmatrix}, \tag{5.3}$$

where the matrix M is defined by

$$M \equiv \begin{pmatrix} 0 & 1 & -1 \\ -1 & 0 & 1 \\ 1 & -1 & 0 \end{pmatrix}.$$

The solution of this system is constrained to move around the circle that is the inter-section of the plane and sphere determined by the conserved quantities $u_0 + u_1 + u_2$ and $u_0^2 + u_1^2 + u_2^2$. Upon denoting the value of the latter quantity by $3\overline{a^2}$, an orbit in the family of period-three oscillations is uniquely determined by the values of $\bar{a}$ and $\overline{a^2}$. Moreover, one can show that for each such orbit

$$\tfrac{1}{3}(u_0u_1 + u_1u_2 + u_2u_0) = \tfrac{1}{2}(3\bar{a}^2 - \overline{a^2}), \tag{5.4}$$

and

$$\frac{1}{T}\int_0^T (u_1u_2(u_1+u_2) + u_2u_0(u_2+u_0) + u_0u_1(u_0+u_1))\,\mathrm{d}t = 6\bar{a}^3, \tag{5.5}$$

where $T = \frac{4}{3}\sqrt{3}\pi h/\bar{a}$ is the period of the orbit.

Now, we derive equations that govern a modulation of this family of exact period-three oscillations. It is natural to introduce the variables

$$v_j = \tfrac{1}{3}(u_{j-1} + u_j + u_{j+1}), \qquad w_j = \tfrac{1}{3}(u_{j-1}^2 + u_j^2 + u_{j+1}^2). \tag{5.6}$$

Both v_j and w_j are locally conserved densities of the scheme (1.2) and are smoothly varying for modulated period-three oscillations. The evolution of v_j and w_j is obtained by averaging the local conservation laws (1.3) over three adjacent spatial points as

$$\frac{\mathrm{d}v_j}{\mathrm{d}t} + \frac{F_{j+1/2} - F_{j-1/2}}{h} = 0, \qquad \frac{\mathrm{d}w_j}{\mathrm{d}t} + \frac{G_{j+1/2} - G_{j-1/2}}{h} = 0, \tag{5.7}$$

where the fluxes are

$$\begin{aligned} F_{j+1/2} &= \tfrac{1}{18}\left(u_{j-1}^2 + u_j^2 + u_{j+1}^2 + u_{j-1}u_j + u_j u_{j+1} + u_{j+1}u_{j+2} + u_j^2 + u_{j+1}^2 + u_{j+2}^2\right), \\ G_{j+1/2} &= \tfrac{1}{9}\left(u_{j-1}u_j(u_{j-1}+u_j) + u_j u_{j+1}(u_j + u_{j+1}) + u_{j+1}u_{j+2}(u_{j+1}+u_{j+2})\right). \end{aligned} \tag{5.8}$$

Now formally pass to the continuum limit. For an exact period-three oscillation the flux F is a constant that can be evaluated using (5.4) as $\frac{1}{4}(\bar{a}^2 + \overline{a^2})$. The flux G on the other hand must be averaged over the rapid time variation using (5.5). One finds that the modulation equation for period-three oscillations are

$$\partial_t v + \tfrac{1}{4}\partial_x(v^2 + w) = 0, \qquad \partial_t w + \tfrac{2}{3}\partial_x v^3 = 0. \tag{5.9}$$

Note that these modulation equations differ from those obtained for period-two oscillations (2.6).

System (5.9) is hyperbolic wherever $v \neq 0$, in which case it is strictly hyperbolic with its characteristic velocities given by v and $-\frac{1}{2}v$. The system has the Riemann invariant form

$$\partial_t(2v^2 + w) + v\partial_x(2v^2 + w) = 0, \qquad \partial_t(w - v^2) - \tfrac{1}{2}v\partial_x(w - v^2) = 0. \tag{5.10}$$

The second equation shows that the region $v^2 \leq w$ is invariant for classical solutions of (5.9), a fact consistent with the origins of v and w. Indeed, if one sets $w = v^2$, which corresponds to there being no oscillations, in (5.9) then v is seen to satisfy the Hopf equation (1.1). The first equation in (5.10) shows that the region $2v^2 + w \geq 0$ is invariant too, but this region is contained in the first.

It is reasonable to expect that classical solutions of (5.9) that satisfy $0 < v^2 \leq w$ will describe the modulation of period-three oscillations so long as they do not develop a singularity. This can be illustrated through numerical experiments. We consider initial data that are period-three oscillations with a long wave length modulation as shown in Fig. 11(a). The numerical solutions of (1.2) at $t = 0.1$, 0.2, and 0.3 are plotted in Figs. 11(b), (c) and (d), respectively. The dynamic nature of period-three oscillations make them hard to observe directly in numerical experiments. However, the averages of u_j and u_j^2 over three adjacent points are slowly varying, thereby making the underlying period-three behavior clear. In Figs. 12(a)–(b) we plot the solution (v, w) of the modulation equations

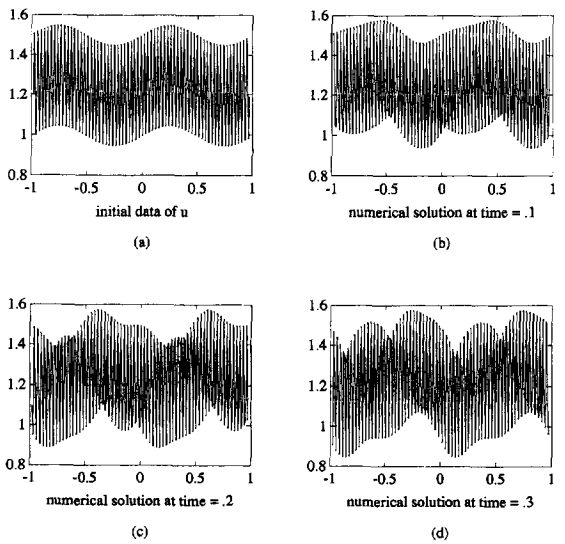

Fig. 11. Modulated period-three oscillations of the dispersive scheme (1.2): (a) the initial data; (b), (c) and (d) the numerical solutions at $t = 0.1$, 0.2 and 0.3, respectively.

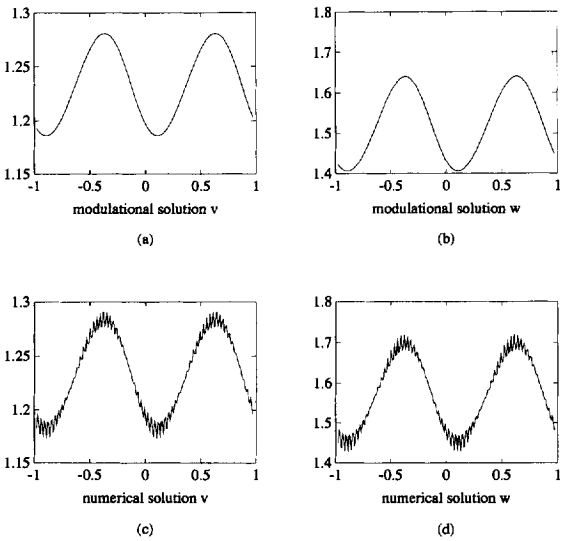

Fig. 12. The modulational behavior of period-three oscillations: (a) and (b) v and w, respectively, from the solution of the modulation equations (4.7); (c) and (d) three point averages of u_j and u_j^2, respectively, of the same solution of the scheme (1.2) shown in Fig. 11.

(5.9) which are solved by a well-resolved Lax–Friedrichs scheme. For comparison, in Figs. 12(c)–(d) we plot the averages over three adjacent points of u_j and u_j^2 from the numerical solution. We can see that the modulation equation give a good description of the modulated period-three solution.

6. Discussion

We have studied modulated oscillatory behavior in solutions of a nonintegrable dispersive numerical scheme that approximates the Hopf equation. Oscillations are generated in the numerical solution when the classical solution of the Hopf equation develops an infinite derivative. In some cases these oscillations are period-two, and we derived a 2×2 system of modulation equations to describe it. The modulation equations are strictly hyperbolic in a region containing nonzero initial data. We showed that, so long as a solution of these equations remains sufficiently regular and inside the strictly hyperbolic region, it describes the weak limit of the modulated period-two oscillations.

More remarkably, we found that some nonsmooth solutions of the modulation equations describe the weak limit near points of transition between regions of nonoscillatory and oscillatory behavior. The matching between these regions was found to be described by a second Painlevé transcendent. These latter results are largely formal or local in nature. Some of the difficulties of trying to rigorously extend the validity of the modulation equations (2.6) in this nonintegrable setting were shown in Section 4. Further evidence for at least some extended validity of modulation theory was given for period-three oscillations. It is hoped that some of these extensions of the validity of modulation theory can be made rigorous.

References

[1] M.J. Ablowitz and J.F. Ladik, Nonlinear differential-difference equations and fourier analysis, J. Math. Phys. 17 (1976) 1011–1018.
[2] A.M. Bloch and Y. Kodama, Dispersive regularization of the Whitham equation for the Toda lattice, SIAM J. Appl. Math. 52 (1991) 909–928.
[3] R. Courant and D. Hilbert, Methods of Mathematical Physics (Wiley, New York, 1962).

[4] B. Engquist and J.-G. Liu, Numerical methods for oscillatory solutions to hyperbolic problems, Comm. Pure Appl. Math. 46 (1993) 1327–1361.
[5] N. Ercolani, S. Jin, C.D. Levermore and W. MacEvoy, The zero dispersion limit of the NLS/mKdV hierarchy for the nonselfadjoint ZS operator, preprint (1993).
[6] H. Flaschka, M.G. Forest and D.W. McLaughlin, Multiphase averaging and the inverse spectral solutions of the Korteweg–de Vries equation, Comm. Pure Appl. Math. 33 (1980) 739–784.
[7] J. Goodman and P.D. Lax, On dispersive difference schemes I, Comm. Pure Appl. Math. 41 (1988) 591–613.
[8] J.M. Greenberg, The shock generation problem for a discrete gas with short range repulsive force, Comm. Pure Appl. Math. 45 (1992) 1125–1139.
[9] M. Hays, C.D. Levermore and P.D. Miller, Macroscopic lattice dynamics, Physica D 79 (1994) 1–15.
[10] B.M. Herbst and M.J. Ablowitz, Numerically induced chaos in the nonlinear Schrödinger equation, Phys. Rev. Lett. 62 (1989) 2065–2068.
[11] B.L. Holian, H. Flaschka and D.W. McLaughlin, Shock waves in the Toda lattice: Analysis, Phys. Rev. A 24 (1981) 2595–2623.
[12] B.L. Holian, G.K. Straub, Molecular dynamics of shock waves in one-dimensional chains, Phys. Rev. B 18 (1978) 1593–1608.
[13] T.Y. Hou and P.D. Lax, Dispersive approximations in fluid dynamics, Comm. Pure Appl. Math. 44 (1991) 1–40.
[14] E.L. Ince, Ordinary Differential Equations (Dover, New York, 1956).
[15] S. Jin, C.D. Levermore and D.W. McLaughlin, The semiclassical limit for the defocusing nonlinear Schrödinger hierarchy, preprint (1994); The behavior of solutions of the NLS equation in the semiclassical limit, in: Singular Limits of Dispersive Waves, eds. Ercolani, Gabitov, Levermore and Serre NATO ASI Series B 320 (Plenum, New York, 1994) pp. 335–355.
[16] M. Kac and P. von Moerbeke, On an explicitly soluble system of nonlinear differential equations related to certain Toda lattices, Adv. in Math. 16 (1975) 160–169.
[17] K. McLaughlin, Ph.D. Dissertation, New York University (1994).
[18] P.D. Miller, N.M. Ercolani, I.M. Krichever and C.D. Levermore, Finite genus solutions to the Ablowitz–Ladik equations, Comm. Pure Appl. Math. 48 (1995) 1369–1440.
[19] P.D. Miller, N.M. Ercolani and C.D. Levermore, Modulation of multiphase waves in the presence of resonance, Physica D 92 (1996) 1–27.
[20] P.D. Lax, On dispersive difference schemes, Physica D 18 (1986) 250–254.
[21] P.D. Lax and C.D. Levermore, The zero dispersion limit of the Korteweg–de Vries equation, Proc. Nat. Acad. Sci. USA 76 (1979) 3602–3606; The small dispersion limit of the Korteweg–de Vries equation I, II, III, Comm. Pure Appl. Math. 36 (1983) 253–290, 571–593, 809–829.
[22] P.D. Lax, C.D. Levermore and S. Venakides, The generation and propagation of oscillations in dispersive IVPs and their limiting behavior, in: Important Developments in Soliton Theory, eds., T. Fokas and V.E. Zakharov (Springer, New York, 1993) pp. 205–241.
[23] C.D. Levermore and J.-G. Liu, Oscillations arising in numerical experiments, in: Singular Limits of Dispersive Waves, eds. Ercolani, Gabitov, Levermore and Serre NATO ASI series B 320 (Plenum, New York, 1994) pp. 329–346.
[24] R. Rosales and C. Turner, The small dispersion limit for a nonlinear semi-discrete system of equations: Part I, Stud. Appl. Math. (1995) submitted.
[25] G. Strang, Accurate partial differential method II, Num. Math. 6 (1964) 37–46.
[26] M. Toda, Theory of Nonlinear Lattices, Series in Solid-State Sciences, Vol. 20, 2nd enlarged Ed. (Springer, New York, 1988).
[27] L. Trefethen, Instability of difference models for hyperbolic initial boundary value problems, Comm. Pure Appl. Math. 37 (1984) 329–367.
[28] S. Venakides, The zero dispersion limit of the Korteweg–de Vries equation with nontrivial reflection coefficient, Comm. Pure Appl. Math. 38 (1985) 125–155; The zero dispersion limit of the Korteweg–de Vries equation with periodic initial data, AMS Trans. 301 (1987) 189–225.
[29] S. Venakides, P. Deift and R. Oba, The Toda shock problem, Comm. Pure Appl. Math. 44 (1990) 1171–1242.
[30] J. von Neumann, Proposal and analysis of a new numerical method in the treatment of hydrodynamical shock problems, Collected Works VI (Pergamon, New York, 1961).
[31] G.B. Whitham, Linear and Nonlinear Waves (Wiley, New York, 1974).
[32] N.J. Zabusky and M.D. Kruskal, Interaction of "solitons" in a collisionless plasma and the recurrence of initial states, Phys. Rev. Lett. 15 (1965) 240–243.